Pergamon

Int. J. Solids Structures Vol. 34, No. 3, pp. 289–296, 1997

0020–7683/97 $15.00 + .00

PII: S0020–7683(96)00009–1

DIVERGING ELASTIC WAVES IN THIN TAPERED PLATES

K. D. TWEET, M. J. FORRESTAL
Sandia National Laboratories, Albuquerque, NM 87185-0303, U.S.A.

and

W. E. BAKER
Department of Mechanical Engineering, University of New Mexico, Albuquerque, NM 87131, U.S.A.

(*Received* 15 *August* 1995; *in revised form* 20 *December* 1995)

Abstract—We studied diverging elastic waves in thin, truncated, tapered plates loaded in the plane of the plates with sine-squared strain pulses. A one-dimensional plane stress model was developed to predict the strain pulses that propagate away from the loaded edges into the linearly increasing plate cross-sections. We conducted experiments with 6.35-mm-thick, 6061-T651 aluminum plates and measured strain-time responses at two locations away from the loaded edges along the plate centerlines. Strain measurements from plates with 6- and 12-degree half-apex angles were compared with predictions from the one-dimensional model. Copyright © 1996 Elsevier Science Ltd.

INTRODUCTION

Graff (1991) presents a comprehensive coverage of the broad field of wave propagation in elastic solids. Those problems most closely related to our study are concerned with elastic wave propagation in truncated solid and hollow cones (Kenner and Goldsmith, 1968; Kenner *et al.*, 1969). Kenner *et al.* (1969) present a one-dimensional, diverging wave model for the in-plane membrane response of a thin, truncated, hollow conical shell and compare predictions with strain measurements. In our study, we present a one-dimensional plane stress model for diverging elastic waves in thin, tapered plates and also compare predictions with strain measurements. Coincidentally, the wave equations for both the hollow cone and tapered plate problems have the same functional form. For the hollow cone problem, Kenner *et al.* (1969) solve the wave equation by taking a Laplace transform and inverting the transformed solution with a numerical evaluation of a Volterra integral equation. For our tapered plate problem, we solved the wave equation by taking a Laplace transform and inverting the transformed equation with the inversion integral and residue theorems. While our solution contains Bessel functions, numerical evaluation of our solution is now straightforward on a personal computer (Wolfram, 1991).

In the following sections, we present the model derivation, describe the experimental design, and show comparisons between predictions and strain-time measurements.

MODEL

Figure 1 shows the truncated plate geometry and coordinates. We derive a linear elastic, one-dimensional plane stress solution for strain waves that propagate in the axial direction x from an input strain pulse applied at $x = a$. The one-dimensional wave equation written in terms of particle displacement u (Graff, 1991; Tweet, 1995) is

$$\frac{\partial^2 u}{\partial x^2} + \frac{1}{x}\frac{\partial u}{\partial x} = \frac{1}{c^2}\frac{\partial^2 u}{\partial t^2} \tag{1}$$

$$c^2 = E/\rho \tag{2}$$

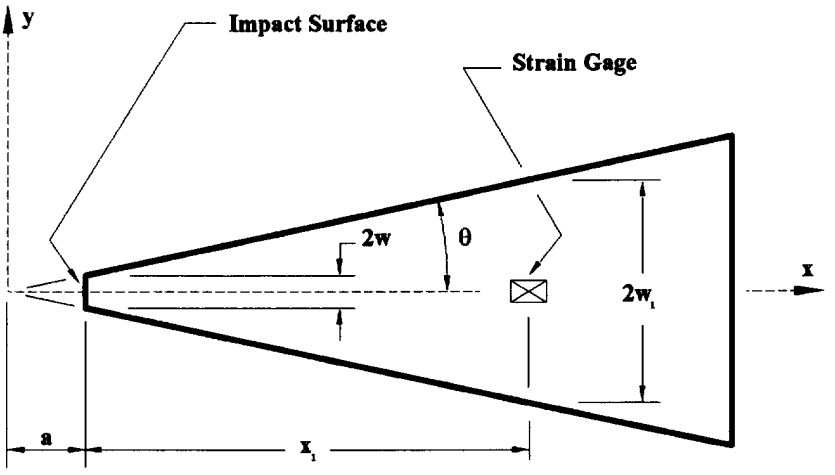

Fig. 1. Truncated plate geometry and coordinates.

where E is Young's modulus, ρ is density, and t is time. In the derivation of eqn (1), we assume that a plane wave propagates in the x-direction (Fig. 1) and that the axial stresses are uniformly distributed across the plate width at each axial position.

For convenience, we introduce the dimensionless axial distance and time

$$\eta = \frac{x}{a}, \quad \tau = \frac{ct}{a} \tag{3}$$

and eqn (1) can be written as

$$\frac{\partial^2 u}{\partial \eta^2} + \frac{1}{\eta}\frac{\partial u}{\partial \eta} = \frac{\partial^2 u}{\partial \tau^2} \tag{4}$$

The particles in the plate are at rest before the plate is loaded, so the initial conditions are

$$u(\eta, 0) = \frac{\partial u}{\partial \tau}(\eta, 0) = 0 \tag{5}$$

We show later in our experimental section that the plate is loaded at $x = a$ or $\eta = 1$ with a nearly sine-squared strain pulse. The sine-squared strain pulse is a good estimate for the experimental load and allows for a convenient analytical solution. Thus, the strain boundary condition is taken as

$$\varepsilon(1, \tau) = \frac{1}{a}\frac{\partial u}{\partial \eta}(1, \tau) = \varepsilon_0 \sin^2(\pi\tau/T), \quad 0 < \tau < T \tag{6a}$$

$$\varepsilon(1, \tau) = \frac{1}{a}\frac{\partial u}{\partial \eta}(1, \tau) = 0, \quad \tau > T \tag{6b}$$

The Laplace transformed solution of eqn (4) for diverging waves is

$$\bar{u}(\eta, z) = B(z)K_0(\eta z) \tag{7}$$

where $\bar{u}(\eta, z)$ is the Laplace transform of $u(\eta, \tau)$, and K_n is a modified Bessel function of the second kind of order n. $B(z)$ is found from the boundary condition given by eqns (6a, b), and the transformed solution for axial strain is given by

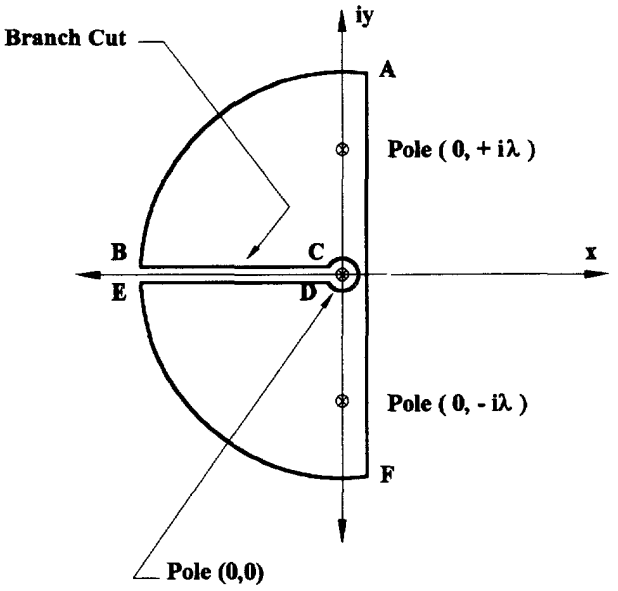

Fig. 2. Contour integration path.

$$\bar{\varepsilon}(\eta, z) = \frac{\varepsilon_0 \lambda^2}{2} \cdot \frac{K_1(\eta z)(1 - e^{-zT})}{z(z^2 + \lambda^2) K_1(z)} \tag{8a}$$

$$\lambda = 2\pi / T \tag{8b}$$

The inverse transform of eqn (8a) is obtained from the inversion integral and residue theorems (Churchill, 1958; Forrestal and Alzheimer, 1968). Figure 2 shows the path of integration. The modified Bessel function, K_1, requires a branch cut along the negative real axis, and Geers (1969) proved that $K_1(z)$ has no poles within the contour. The three poles within the contour are located at $z = 0$ and $z = \pm i\lambda$. Thus, axial strain is given by

$$\frac{\varepsilon(\eta, \tau)}{\varepsilon_0} = F(\eta, \tau) H(\tau) - F(\eta, \tau - T) H(\tau - T) \tag{9a}$$

$$F(\tau) = \frac{1}{2\eta} - \frac{[J_1(\eta\lambda) J_1(\lambda) + Y_1(\eta\lambda) Y_1(\lambda)]}{2[J_1^2(\lambda) + Y_1^2(\lambda)]} \cos \lambda\tau - \frac{[Y_1(\eta\lambda) J_1(\lambda) - J_1(\eta\lambda) Y_1(\lambda)]}{2[J_1^2(\lambda) + Y_1^2(\lambda)]} \sin \lambda\tau$$
$$+ \frac{\lambda^2}{2} \int_0^\infty \frac{[I_1(\eta r) K_1(r) + I_1(r) K_1(\eta r)] e^{-r\tau}}{[K_1^2(r) + \pi^2 I_1^2(r)][r(r^2 + \lambda^2)]} dr \tag{9b}$$

where J_1, Y_1 are Bessel functions of the first and second kind of order one; I_1, K_1 are modified Bessel functions of the first and second kind of order one; λ is given by eqn (8b); and $H(\tau)$ is the Heaviside unit function. In eqn (9b), the first term is the contribution from the pole at the origin, the second and third terms are contributions from poles at $z = \pm i\lambda$, and the integral term is the contribution from the branch cut along the negative real axis. To obtain eqn (9b), we used the equations given by McLachlan (1961) that give the real and imaginary parts of $K_1(z)$ in terms of other Bessel functions. While eqn (9b) contains Bessel functions, numerical evaluation is straightforward with a personal computer (Wolfram, 1991).

Equations (9a, b) predict the strain wave response that propagates away from the loaded plate edge at $\eta = 1$ in terms of the dimensionless variables η and τ given by eqn (3). At first glance, the strain response appears independent of the half-apex, θ, shown in Fig. 1. However, Fig. 1 shows the loaded edge of the tapered plate at $x = a$ has a plate width $2w$, so

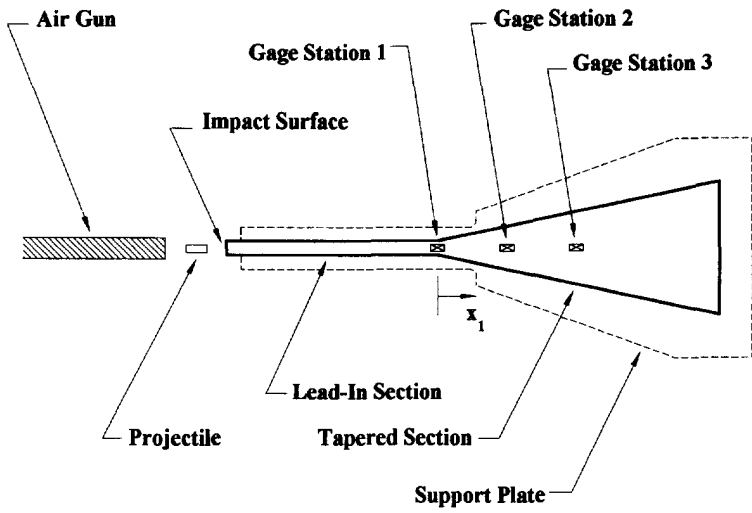

Fig. 3. Experimental arrangement.

$$w = a\tan\theta \tag{10}$$

In addition, the axial location for a strain gage shown in Fig. 1 will be given from the edge of the plate at $x = a$, so it is necessary to define distance from the loaded edge of the plate as

$$x_1 = x - a \tag{11}$$

The width of the plate at x_1 is defined as $2w_1$, where

$$w_1 = w + x_1\tan\theta \tag{12}$$

We can now relate the coordinates convenient for laboratory measurements to the dimensionless coordinates used in the model. Substituting eqns (10, 11) into eqn (3) gives

$$\eta = 1 + \frac{x_1\tan\theta}{w}, \quad \tau = \frac{ct\tan\theta}{w} \tag{13}$$

EXPERIMENTAL DESIGN

Figure 3 shows the experimental arrangement. The test plates were machined from 6.35-mm-thick, 6061-T651 aluminum sheets and consisted of a lead-in section and a tapered section. The rectangular lead-in section has width 25.4 mm and length 381 mm. The tapered sections have half-apex angles $\theta = 6$ and 12 degrees and length 508 mm. The dashed line in Fig. 3 represents the support plate. Four 6.35-mm-diameter steel ball bearings were placed in countersunk holes on the top surface of the support plate, and the test plate was placed on the ball bearings.

Three pairs of strain gages (BLH FAB-06N-12S6) were bonded to the top and bottom surfaces of the test plates along the plate centerlines. The averages of the axial strain-gage pairs were recorded in order to eliminate bending effects. Strain gage locations are measured from the start of the tapered section with coordinate x_1 shown in Fig. 3. The first strain

Table 1. Strain gage locations for the $\theta = 6$ degree plate

Gage station	x_1 (mm)	η	$2w_1$ (mm)
1	0	1.0	25.4
2	96.8	1.8	45.7
3	254	3.1	78.7

Table 2. Strain gage locations for the $\theta = 12$ degree plate

Gage station	x_1 (mm)	η	$2w_1$ (mm)
1	0	1.0	25.4
2	125	3.1	78.7
3	251	5.2	132

gage pair is located at $x_1 = 0$. Tables 1 and 2 list the downstream locations, the dimensionless spatial variable η, and the plate width at gage locations.

We show later that nearly sine-squared strain pulses were recorded at the start of the tapered plate ($x_1 = 0$ in Fig. 3). These strain pulses were generated by launching a projectile at the lead-in section of the test plate. To obtain the desired strain pulse at $x_1 = 0$, a 0.10-mm-thick rectangular piece of plastic* was attached to the impact end of the lead-in bar with a thin layer of vacuum grease. A 14.3-mm-diameter, 6061-T651 aluminum projectile with length 38.1 mm was launched from a gas gun and struck the lead-in bar. A strain wave propagated down the lead-in section towards the tapered section. The lead-in section is 381 mm long, so there was ample distance for the strain pulse to become uniformly distributed over the lead-in cross-section prior to arrival at $x_1 = 0$, the start of the tapered section. In addition, the lead-in section and the tapered plate lengths were long enough that reflected strain pulses from the ends occur after the time durations of interest for the strain measurements downstream on the tapered plates.

We designed the experiments to limit our instrumentation to strain gage pairs. The strain-time history at the start of the tapered plate $x_1 = 0$ in Fig. 1 is the input to our tapered plate model. In the next section, we compare model predictions and strain measurements at two stations along the centerline of the diverging, tapered plate.

MODEL PREDICTIONS AND STRAIN MEASUREMENTS

Tweet (1995) conducted six sets of experiments for plates with 6- and 12-degree half-apex angles. These experiments showed only minor differences in the measured strain-time histories among the six sets of experiments for each plate. Figures 4 and 5 show model predictions and strain measurements for the 6- and 12-degree plates, respectively. The experiments were designed to produce a nearly sine-squared input strain pulse at $x_1 = 0$ shown in Fig. 3 (gage station 1 in Tables 1 and 2). Figures 4a and 5a show the input strain pulses and the analytical curve-fits given by eqns (6a, b). The measured input strain pulse is denoted by the solid curve and the analytical fit is given by the dashed curve. The analytical fits are in excellent agreement with strain measurements for about 27 μs. Thus, the accuracy of the model should be judged only for the first 27 μs for comparison between predictions and data at the downstream stations of the tapered plates.

Each data channel was triggered independently using an integral trigger; therefore, the time correlation among the three data channels is not known. Zero times in Figs 4 and 5 correspond to the arrival time of the wave front at the gage stations, determined by the first bit deviation from baseline voltage. Additionally, the predicted strain responses were adjusted so the peak values occurred at the same time as the peaks in the strain measurements.

* IR 1140 transparency film manufactured by 3M Corporation.

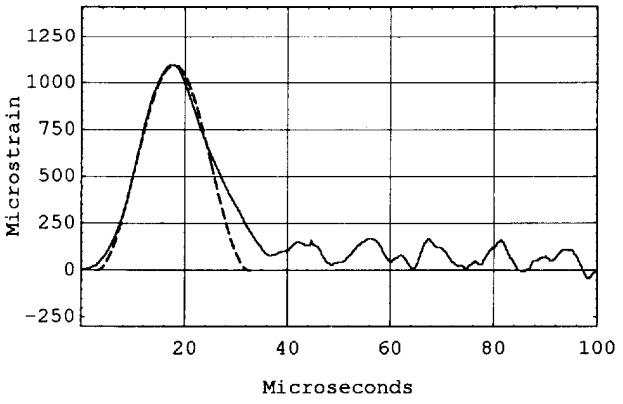

(a) Input Strain Pulse at Station 1

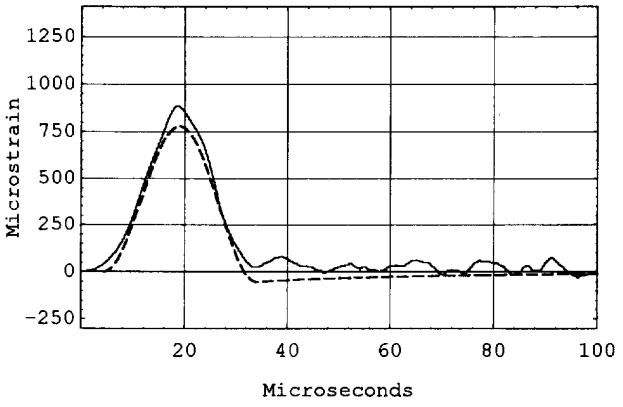

(b) Strain Response at Station 2

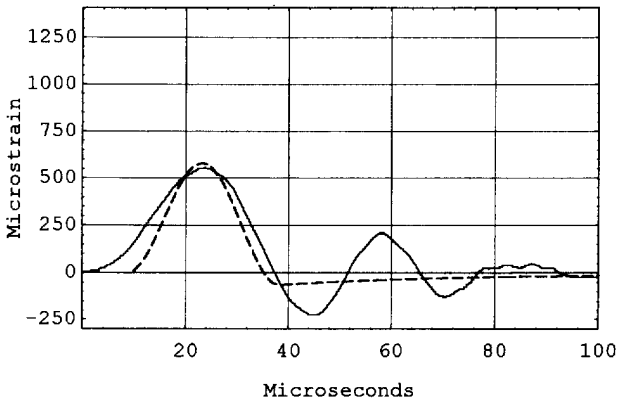

(c) Strain Response at Station 3

Fig. 4. Model predictions (dashed lines) and strain data (solid lines) for the $\theta = 6$ degree plate.

Figure 4 shows results for the input strain pulse and strain pulses for two stations downstream for the plate with a 6-degree half-apex angle. The attenuation in peak strain with increasing x_1 occurs because the plate width $2w_1$ increases with increasing x_1. As listed in Table 1, $x_1 = 96.8$ mm and 254 mm for gage stations 2 and 3, respectively. Over a time duration of 27 μs, predictions and measurements are in reasonably good agreement. The model predicts a lower amplitude at station 2 and a shorter pulse duration at station 3.

Figure 5 shows results for the input strain pulse and strain pulses for two stations downstream for the plate with a 12-degree half-apex angle. As listed in Table 2, $x_1 = 125$ mm and 251 mm for the gage stations 2 and 3, respectively. A comparison of Figs 4 and 5

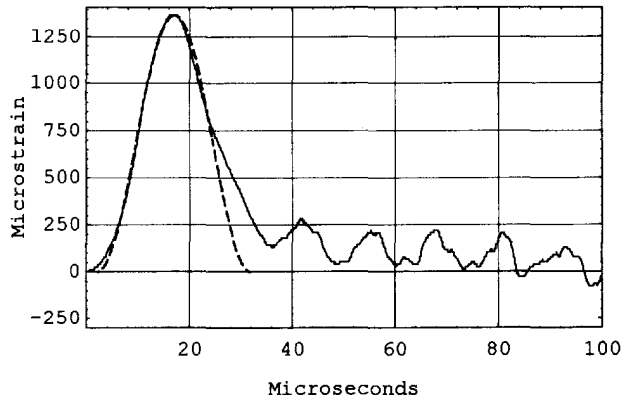

(a) Input Strain Pulse at Station 1

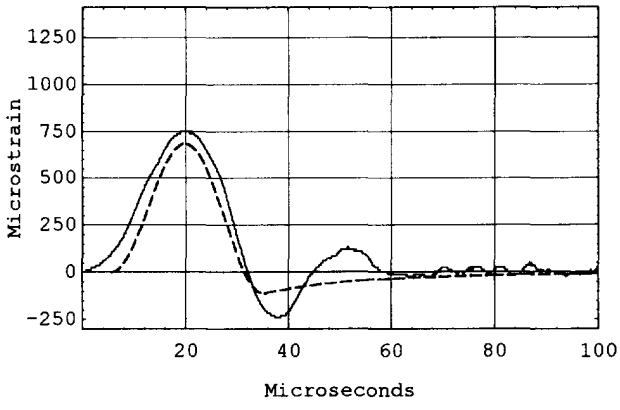

(b) Strain Response at Station 2

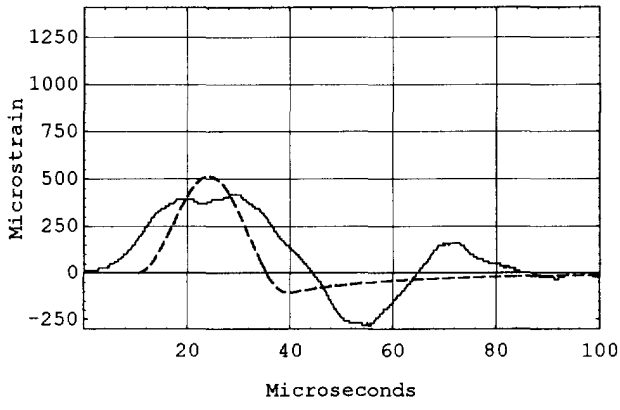

(c) Strain Response at Station 3

Fig. 5. Model predictions (dashed lines) and strain data (solid lines) for the $\theta = 12$ degree plate.

shows that deviations between model predictions and measurements increase as the half-apex angle increases from 6 to 12 degrees. For the 12-degree plate, Fig. 5b shows reasonable agreement at station 2, but the comparisons shown in Fig. 5c for station 3 differ considerably.

Model predictions are in good agreement with strain data for the 6-degree plate at station 2. As x_1 or θ (Fig. 1) increases, differences between model predictions and strain measurements increase. Figures 4 and 5 quantify these trends. As previously discussed, the one-dimensional model assumes that a plane wave propagates in the axial direction. Thus, our model assumes that stresses are uniformly distributed over each plate cross-section.

Since we measure only strain-time histories at the plate centerline, our experiments do not check the uniform stress assumption. We speculate that this uniform stress assumption in the model development is the reason for lack of agreement between predictions and measurements as x_1 or θ increases. We recommend that future experiments use full field measurement techniques to investigate stress distributions (Mason *et al.*, 1994).

SUMMARY

We developed a one-dimensional model to predict strain pulses that propagate away from the loaded edge of truncated plates and into linearly increasing plate cross-sections. Comparisons of model predictions show good agreement for small apex angles. As the apex angles and the distances from the loaded edge increase, the model accuracy decreases.

Acknowledgements—The work performed by K. D. Tweet and M. J. Forrestal was supported by the U.S. Department of Energy under contract DE-AC04-94AL85000.

REFERENCES

Churchill, R. G. (1958). *Operational Mathematics*, McGraw-Hill, New York.

Forrestal, M. J. and Alzheimer, W. E. (1968). Transient motion of a rigid cylinder produced by elastic and acoustic waves. *J. Appl. Mech.* **35,** 134–138.

Geers, T. L. (1969). Excitation of an elastic cylindrical shell by a transient acoustic wave. *J. Appl. Mech.* **36,** 459–469.

Graff, K. F. (1991). *Wave Motion in Elastic Solids*, Dover Publications, New York.

Kenner, V. H. and Goldsmith, W. (1968). Elastic waves in truncated cones. *Experimental Mech.* **8,** 442–449.

Kenner, V. H., Goldsmith, W. and Sackman, J. L. (1969). Longitudinal impact on a hollow cone. *J. Appl. Mech.* **36,** 445–450.

Mason, J. J., Rosakis, A. J. and Ravichandran, G. (1994). Full field measurements of the dynamic deformation field around a growing adiabatic shear band at the tip of a dynamically loaded crack or notch. *J. Mech. Phys. Solids* **42,** 1679–1697.

McLachlan, N. W. (1961). *Bessel Functions for Engineers*, Oxford University Press, London.

Tweet, K. D. (1995). Diverging elastic waves in thin tapered plates. Thesis submitted in partial fulfillment for the Degree of Master of Science in Mechanical Engineering, University of New Mexico, Albuquerque, NM.

Wolfram, S. (1991). *Mathematica*, Addison-Wesley, Reading, MA.